PNAS RESEARCH ARTICLE | EARTH, ATMOSPHERIC, AND PLANETARY SCIENCES OPEN ACCESS

Contribution of anthropogenic aerosols to persistent La Niña-like conditions in the early 21st century

Yen-Ting Hwang[a,1], Shang-Ping Xie[b], Po-Ju Chen[a,c], Hung-Yi Tseng[a], and Clara Deser[d,1]

Contributed by Clara Deser; received September 8, 2023; accepted December 8, 2023; reviewed by Kay McMonigal and Michael J. McPhaden

The discrepancy between the observed lack of surface warming in the eastern equatorial Pacific and climate model projections of an El Niño-like warming pattern confronts the climate research community. While anthropogenic aerosols have been suggested as a cause, the prolonged cooling trend over the equatorial Pacific appears in conflict with Northern Hemisphere aerosol emission reduction since the 1980s. Here, using CESM, we show that the superposition of fast and slow responses to aerosol emission change—an increase followed by a decrease—can sustain the La Niña-like condition for a longer time than expected. The rapid adjustment of Hadley Cell to aerosol reduction triggers joint feedback between low clouds, wind, evaporation, and sea surface temperature in the Southeast Pacific, leading to a wedge-shaped cooling that extends to the central equatorial Pacific. Meanwhile, the northern subtropical cell gradually intensifies, resulting in equatorial subsurface cooling that lasts for decades.

climate change | atmosphere–ocean interaction | climate teleconnection | sea surface temperature pattern

Significance

The tropical Pacific plays a crucial role in global energy and moisture distribution, and accurate prediction of its changes is vital for society's adaptation to growing climate change. The cause of surface cooling trends observed over the past 40 y in the tropical eastern Pacific eludes a satisfactory explanation. Our study shows that anthropogenic aerosol effects on the equatorial Pacific Ocean may have reached a peak and that the response features a La Nina-like cooling pattern. Prolonged aerosol influence is clarified through dual timescale responses involving air–sea flux and ocean dynamics.

The sea surface temperature (SST) anomaly pattern in the tropical Pacific has significant influence on global weather and climate. Over the past four decades, the equatorial cold tongue has cooled while the rest of the tropics have warmed (1), modulating the pace of global surface warming (2, 3), amplifying tropical cyclone genesis over the Northwest Pacific (4), and heightening the likelihood of drought occurrence in the western United States (5). The aforementioned trends might cease or even reverse if the cold tongue warms up and Walker Cell weakens, as anticipated by climate models. How the tropical Pacific may change under anthropogenic forcing has been a subject of active debate for decades and is still ongoing. The complex interplay among global dynamics, air–sea interactions, and radiative processes has given rise to multiple unresolved conundrums, including the interpretation of the observed trend, the discrepancy between models and observations (1, 6), and diverging theories (6, 7).

One plausible interpretation for the observed eastern tropical Pacific cooling trend, particularly during the early 2000s, is that it is predominantly driven by internal variability, either through the negative phase of Pacific Decadal Variability (PDV) (2, 8–13) or the decadal variation of independent ENSO events (14–16). Despite accounting for a range of internal variability, it remains uncommon to find historical simulations with fully coupled climate models that accurately replicate the strengthening of the zonal SST gradient observed over the past 50 y (1, 6). Furthermore, the cooling trend observed in the subtropical South Pacific and equatorial eastern Pacific has persisted despite the transition toward a positive PDV phase after 2013, prompting the need for an alternative explanation, namely that a portion of the observed trend may be driven by external forcing that current models fail to simulate adequately.

The exploration of idealized experiments, which enable the decomposition of the complex response to increasing carbon dioxide (CO_2) into a fast and a slow component, has yielded significant insights (17–19). The fast component closely aligns with the observed trend (20) and the "ocean thermostat" hypothesis (21). This stands in stark contrast to the slow component, which exhibits a reduced zonal gradient consistent with long-term model projections and the thermodynamic constraints imposed by radiative cooling (22) and evaporative damping (23, 24). The framework of multiple timescale responses offers a promising avenue for resolving discrepancies between models and observations, as well as reconciling the various competing mechanisms at play in this intricate system (19, 25). It is hypothesized that the strength of the ocean thermostat may be underestimated by current models, and the enhanced warming over the equatorial cold tongue may eventually manifest (19, 25).

Evidence from single forcing experiments indicates that anthropogenic aerosols exert a comparable influence to greenhouse gases in shaping the SST pattern during the

Author affiliations: [a]Department of Atmospheric Sciences, National Taiwan University, Taipei 10617, Taiwan; [b]Scripps Institute of Oceanography, University of California San Diego, La Jolla, CA 92093; [c]Department of Atmospheric, Oceanic, and Earth Sciences, George Mason University, Fairfax, VA 22030; and [d]Climate and Global Dynamics Division, National Center for Atmospheric Research, Boulder, CO 80305

Author contributions: Y.-T.H. designed research; P.-J.C. and H.-Y.T. performed research; C.D. contributed new reagents/analytic tools; Y.-T.H., P.-J.C., and H.-Y.T. analyzed data; S.-P.X. provided important insights for interpreting the results and forming the article's storyline; C.D. provided important insights for interpreting the results; and Y.-T.H., S.-P.X., and C.D. wrote the paper.

Reviewers: K.M., University of Alaska Fairbanks; and M.J.M., National Oceanic and Atmospheric Administration Pacific Marine Environmental Laboratory.

The authors declare no competing interest.

[1]To whom correspondence may be addressed. Email: ythwang@ntu.edu.tw or cdeser@ucar.edu.

This article contains supporting information online at https://www.pnas.org/lookup/suppl/doi:10.1073/pnas.2315124121/-/DCSupplemental.

Published January 22, 2024.

observational period (26–32). However, our current understanding of the Earth system's responses to anthropogenic aerosols on different timescales remains limited (33), hindering our ability to accurately attribute past climate change and assess uncertainties in climate change projections. For instance, a notable reduction in aerosol concentrations has already been observed in North America and Europe since 1980, as well as in East Asia since 2000. Naively predicting that the decrease in aerosols would lead to a weakening of the observed La Niña-like SST pattern trend appears to contradict both the available observational records and the outcomes of single forcing simulations.

In the following, we explore the possible role of non-monotonic evolution of anthropogenic sulfate aerosols in slowing down the equatorial Pacific warming. Our findings reveal that the equatorial Pacific response to aerosol radiative forcing exhibits distinct fast and slow components. We then put forth a hypothesis that these components interact and result in an equatorial cooling that is stronger in the early 21st century than in the 1980s. The superposition of the fast and slow response to the Northern Hemisphere sulfate aerosol emission trajectory, which consists of an increase followed by a decrease, may sustain the La Niña-like SST pattern for an extended duration that is longer than previous estimations.

The Experimental Design

We differentiate the fast and slow components of the climate system's response to anthropogenic aerosols by conducting a 15-ensemble-member step function experiment using the Community Earth System Model version 1 (CESM1) at 2° resolution for the atmosphere and land components and 1° resolution for the ocean and sea ice components. The last-millennium ensemble (34) and the CMIP5 archive also utilized the same version and resolution, identified as "CESM1 (CAM5.1, FV2)." Note that the CESM1 model at 2° resolution is particularly skillful in simulating some of the key processes involved in the response, including low cloud-SST feedback (35) and the Pacific mean state (36). The experiment consists of suddenly introducing and then maintaining a constant pattern of sulfate aerosol emissions representative of 1980s levels taken from CMIP5 historical forcing data (*SI Appendix*, Fig. S1*A*) for the first 30 y of the simulation, followed by an abrupt return to pre-industrial (year 1850) levels for an additional 30 y. Ensemble members are generated by initializing the experiments by the conditions on January 1st of the last 15 consecutive years in the control simulation. The evolving forced response anomaly is calculated by subtracting the climatology of the 90-y pre-industrial control simulation from the average of the 15 ensemble members. Detailed definitions for the fast and slow components of aerosol emission and aerosol removal can be found in the *Methods*. The fast and slow components of the SST response are very similar to those obtained with a similar set of experiments using the 2020s distribution of sulfate aerosol emissions (*SI Appendix*, Fig. S1 *D* and *F*). The similarity implies that the proposed mechanisms shaping the fast and slow components of SST response are operating across both historical simulations and future projections, despite the different patterns of aerosol emissions.

Multiple Timescale Responses in the Equatorial Pacific Region

The equatorial Pacific, located far from the Northern Hemisphere aerosol emission source regions, shows a clear indication of a multiple timescale response. The imposed step-function in aerosol emissions results in a complex evolution of oceanic temperatures, as shown in Fig. 1. Initially (within the first 3 y), SSTs in the central and eastern equatorial Pacific SST undergo warming before transitioning to cooling thereafter (Fig. 1*A*). It is notable that the maximum cooling takes place in the 3 y immediately following the abrupt cessation of aerosol forcing at year 30 (Fig. 1*A*). Although the surface cooling gradually decreases after year 35, subsurface cooling persists for decades after the radiative forcing has been removed (Fig. 1*B*). Additionally, the subsurface cooling reaches maximum strength during years 33 to 45, after the aerosol emissions return to preindustrial levels. Both the surface and subsurface signals indicate a persistent cooling long after the aerosol emissions are abruptly terminated.

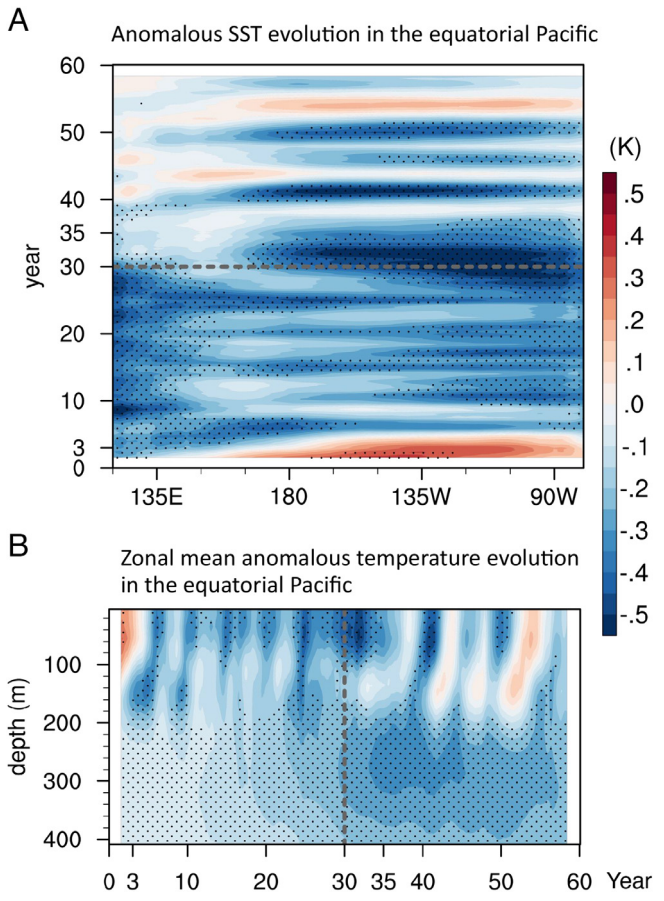

Fig. 1. Temporal evolutions of anomalous oceanic temperature in the idealized aerosol experiments relative to the climatology in the control simulation. (*A*) The 3-y running mean of meridionally averaged SST anomalies in the equatorial Pacific (5°S~5°N). (*B*) The 3-y running mean of the equatorial Pacific temperature response which is zonally and meridionally averaged (5°S~5°N; Pacific basin). Dotted region indicates statistically significant values of temperature anomalies at the 95% confidence level based on two-sided *t* test.

The multiple timescale responses identified in the idealized experiments can also be seen in a more realistic setting. Fig. 2 compares the Niño3.4 index and subsurface ocean temperature in the equatorial Pacific for both the idealized step function experiment and the standard CESM experiments with realistic emission scenarios (historical and RCP8.5) (29) (*Methods*). The average global aerosol emission reaches its highest point around 1970 to 1990, causing the Niño3.4 region's SST and subsurface temperature to experience cooling that show little sign of weakening even after year 1990. The equatorial subsurface cooling reaches maximum strength several decades after the aerosol emissions peak. According to the CESM single forcing experiment, we are about to experience the peak equatorial subsurface cooling (around year 2030 to 2050) induced by aerosols.

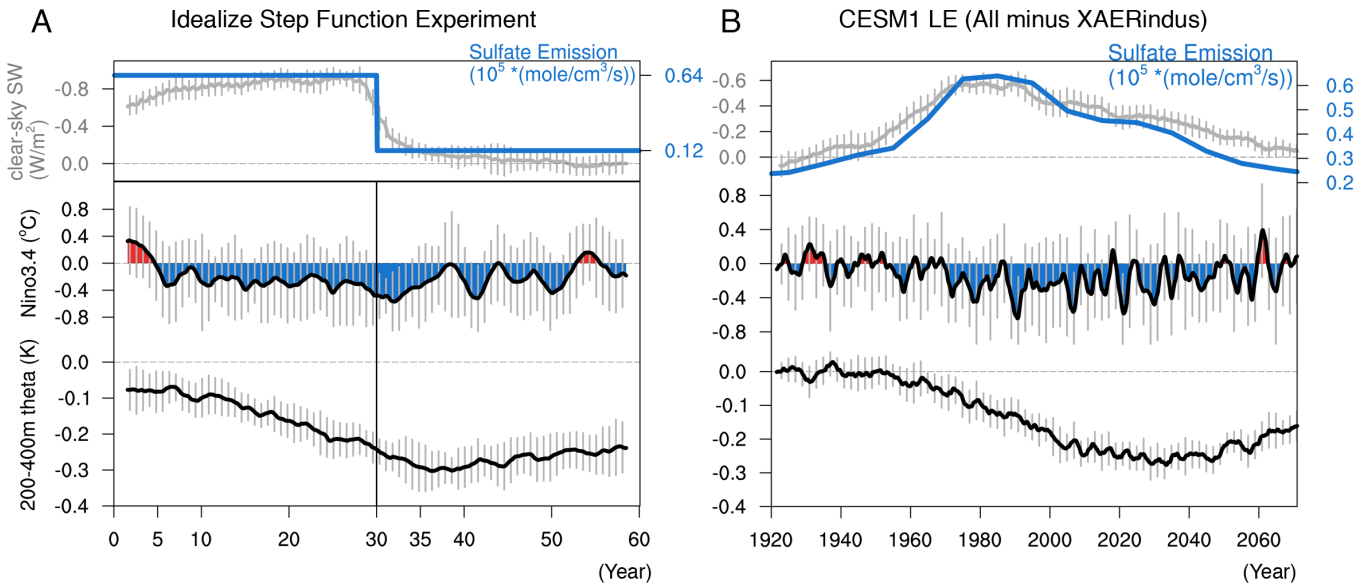

Fig. 2. Temporal evolutions of imposed sulfate aerosol emissions and equatorial Pacific climate response. *Top* row: the global mean sulfate emission imposed in the idealized experiment (*A*) and CESM LE All minus XAERindus (*B*). The gray lines denote the global mean anomalous SW radiation in clear sky. *Middle* and *Bottom* rows: the evolutions of averaged SST in the Niño3.4 region (5°S~5°N; 170°W~120°W) and averaged potential temperature in the subsurface equatorial Pacific (200 to 400 m; 5°S~5°N; Pacific basin) in the idealized experiment (*Left*) and CESM-LE (*Right*). All indices except the global mean sulfate emission are smoothed by 3-y running mean in the idealized experiment and by a 5-y running mean in CESM-LE. The thick black curves and the thin gray bars indicate the ensemble mean and the 1 SD among ensemble members, respectively.

In the following, we utilize the idealized experiment to investigate the distinct characteristics and underlying mechanisms behind the fast and slow elements of the climatic response to anthropogenic aerosol forcing. The multiple timescale elements explain why the peak aerosol influence on the tropical Pacific occurs after emission reduction.

The Fast Component

The fast component reveals a remote influence of aerosols that has the opposite sign from that expected from the imposed forcing, a phenomenon that has yet to be recognized in the existing literature. In the case of aerosol emissions, this manifests as a wedge-shaped SST warming pattern reaching its maximum intensity in the central equatorial Pacific, extending southeastward, and featuring a sharp front north of the equator (Fig. 3*A*). The reduced equatorial zonal SST gradient and easterlies are associated with a flatten thermocline and a typical seesaw temperature anomaly in the equatorial band (Fig. 3*C*). Here, we disentangle how the anomalous radiative forcing, primarily concentrated in the northern extratropics, gives rise to a remote SST response in the equatorial Pacific with an opposite sign from that expected from the forcing. In the *Summary and Outlook*, we will discuss how the same pattern with reversed sign explains the enhanced cooling

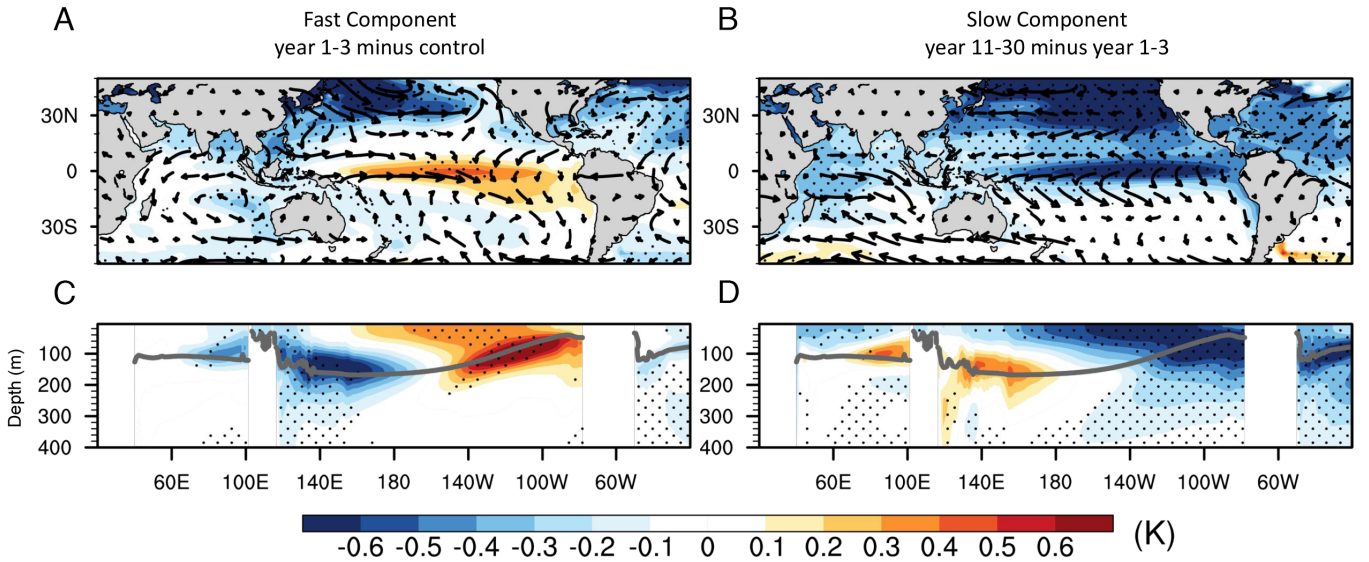

Fig. 3. The fast and slow responses in the idealized aerosol experiments. (*A* and *B*) Spatial patterns of SST (shaded) and surface wind stress (vector) anomalies. (*C* and *D*) Vertical structure of potential temperature anomalies along the equator (5°S~5°N mean) as a function of depth (m). Dotted region indicates statistically significant values of temperature anomalies at the 95% confidence level based on two-sided *t* test.

that takes place after the sudden removal of aerosol emissions in our idealized experiment and contributes to the La Niña-like trend in more realistic simulations (and by extension the observed trends).

We propose that the formation of the cross-equatorial Hadley Cell, along with its associated air–sea interactions, drives the observed teleconnection pattern in the tropical Pacific. The energetic framework (37–39) offers a plausible interpretation for the development of this anomalous cross-equatorial cell. In response to aerosol emissions, an anomalous cross-equatorial cell emerges, transporting energy toward the north (Figs. 4 *A* and *B* and 5*A*). The accompanying pattern of surface winds plays a pivotal role in establishing the SST pattern in the tropical Pacific, as described below.

First, the meridional winds in the equatorial eastern Pacific hold a significant influence over thermocline depth and the strength of the cold tongue (40). A reduction in the trade winds across the equator suppresses mixing, limits upwelling, and results in a flatter thermocline (Fig. 3*C*). Despite very little radiative forcing in the tropics, the anomalous cross-equatorial winds that are generated remotely by aerosols in the northern extratropics can induce a tropical SST response that resembles the dynamical thermostat mechanism frequently discussed in the context of greenhouse warming or volcanic eruptions (19, 21, 25, 41, 42). We confirm the key role of extratropical aerosols via performing additional experiment that only considers tropical aerosol emissions, which does not enable the dynamical thermostat mechanism and displays a slight equatorial cooling instead for the fast response [see *SI Appendix*, Fig. S2, contrary to the hypothesis presented in Verma et al. (33) based on year 2000 emissions].

Second, the anomalous cross-equatorial winds strengthen the trade winds in the northern tropics and weaken them in the southern tropics. Weakened trades in the south inhibit coastal upwelling, diminish stratus and stratocumulus clouds along the coast of South America, and reduce the east-west SST gradient in the subtropics. Given that the climatological rainband is located north of the equator, the combined wind-evaporation-SST and low cloud-SST feedbacks can spread anomalous warming from the Southeast Pacific to the equatorial central and eastern Pacific (43–46) (Fig. 3*A*). Meanwhile, the anomalous cooling caused by strengthened trades and the joint wind-evaporation-low cloud-SST feedback is blocked by the rainband. It can only enter the equatorial region from the west. The resulting weakened zonal SST gradient in the equatorial western-central Pacific reduces the easterlies, thereby reducing zonal cold advection and meridional Ekman energy divergence. This, in turn, further amplifies the warming (47) (see Fig. 4*D* for the anomalous deep tropical subtropical cell (STC) driving the Ekman energy convergence and *SI Appendix*, Fig. S3 for the energy budget analysis of the upper 0 to 50 m).

The Slow Component

The slow component of the climate response to aerosol forcing exhibits an enhanced equatorial zonal SST gradient and an intensification of the Walker Cell, consistent with the literature (26, 28, 48) (Fig. 3*B*). The cooling of the slow component extends well below the thermocline to at least 400 m depth. Intriguingly, these surface and subsurface cooling anomalies in the equatorial region occur within decadal timescale and show little sign of recovery after aerosol removal (Fig. 1), a phenomenon previously unreported in the literature. In this section, we delve into the ocean dynamical mechanisms that drive the spread of aerosol-induced cooling to the equatorial region. The persistent nature of this oceanic response emphasizes the potential to detect the cooling anomalies in the noisy observational records, which we compare with the historical simulations in the last section.

We propose that the interhemispherically asymmetric surface wind anomalies and the associated air–sea interactions in the fast response drive the slow oceanic adjustments and set the stage for

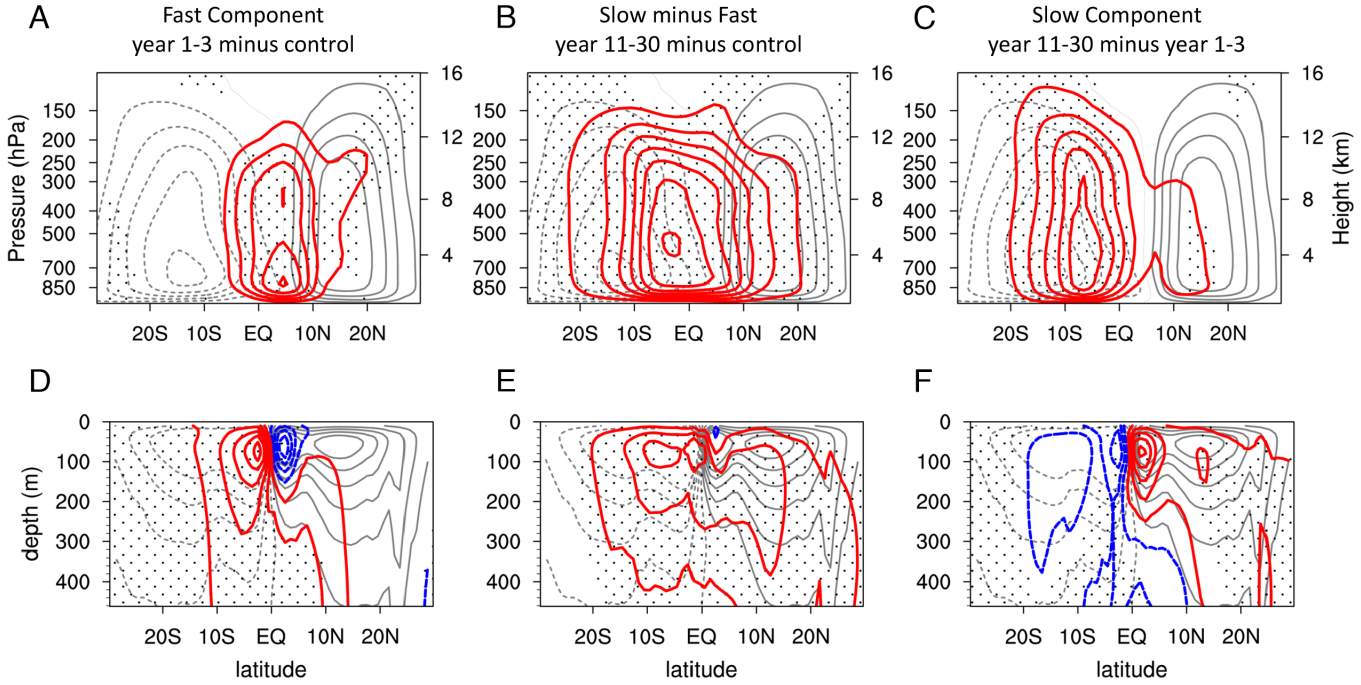

Fig. 4. Climatological (gray contours) and anomalous (colored contours) meridional mass streamfunction in the atmosphere (*A*–*C*) and in the Indo-Pacific ocean (*D*–*F*). Dotted region indicates statistically significant values of anomalies at the 95% confidence level based on two-sided *t* test. The contour intervals for panels (*A*–*C*) are 2×10^{10} m^3/s for climatology and 2×10^9 m^3/s for anomalies. For (*D*–*F*), the contour intervals are 4 Sv for climatology and 0.8 for anomalies.

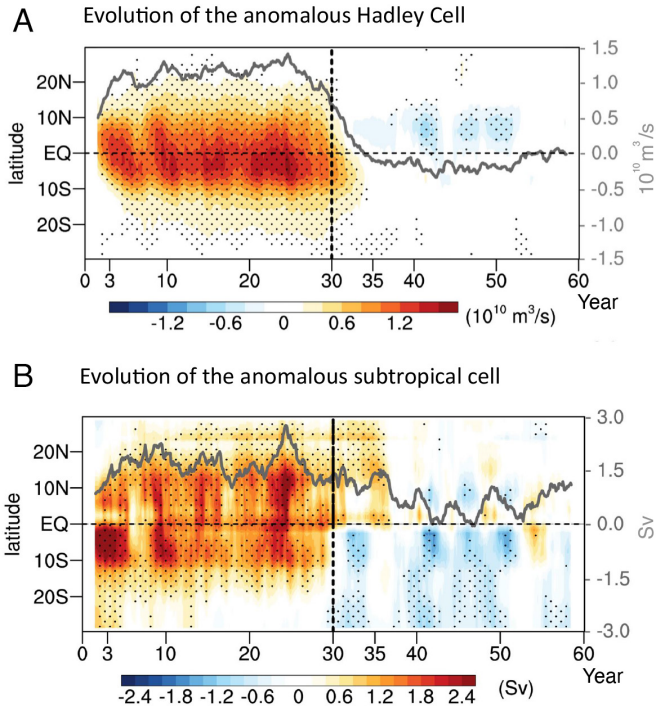

Fig. 5. Temporal evolutions of anomalous meridional circulations and their indices in the idealized aerosol experiments. The timeseries are all smoothed by a 3-y running mean. (*A*) displays the change in Hadley Cell (shaded) which is shown by the vertically averaged mass streamfunction (globally zonal mean; 300 to 700 hPa). The positive anomalies indicate anomalous northward flows in the upper level and southward flows in the lower level, vice versa. The solid line denotes the strength of anomalous cross-equatorial Hadley Cell using the mass streamfunction averaged over the domain (10°S~10°N; 300 to 700 hPa). (*B*) displays the change in the Meridional Overturning Circulation in the tropical Pacific (shaded) through the vertically averaged mass streamfunction (100 to 300 m). The solid line represents the index of the strength which is the maximum of the Meridional Overturning Circulation in a domain (10°N~30°N; 0 to 400 m). Dotted region indicates statistically significant values of anomalous mass streamfunction at the 95% confidence level based on two-sided *t* test.

the slow response. Since oceanic temperature and circulation respond slowly, the resulting equatorial cooling does not become significant until year 10 (Fig. 1*A*). Also, the removal of the aerosol forcing does not result in an immediate recovery of oceanic circulation, as shown below.

The so-called "oceanic tunnel" provides a linkage for the Northern Hemisphere extratropical SST cooling of the fast response to the tropical ocean (45, 49, 50). That is, the aerosol cooling and the associated joint low cloud-WES feedback lower the temperature of waters subducted within the STC, causing colder water to be advected downward and equatorward. Indeed, we observe cooler water penetrating into the oceanic interior in the eastern Pacific basin around 20~30°N and transporting equatorward to 15°N a few years after the imposition of aerosol forcing (*SI Appendix*, Fig. S4).

Targeting the equatorial Pacific oceanic energy budget, the loss of energy and the resultant cooling in the equatorial Pacific Ocean are mainly caused by changes in the northern STC (refer to *SI Appendix*, Fig. S5 for changes in meridional energy convergence dominating energy budgets of 0 to 200 m and 0 to 400 m and see *SI Appendix*, Fig. S6 for $V'\overline{T}$ of the northern boundary outweighing other terms). The cooling in the northern mid-latitudes leads to an increase in subtropical wind stress and wind-stress curl, which then spins up the Pacific Gyre circulation and, as a result of the Sverdrup balance, strengthens the northern STC (Figs. 4*E* and 5*B*). The northern STC intensifies within 2 to 3 y of imposing aerosol forcing, matching the time for baroclinic Rossby waves to cross the Pacific Basin (51, 52). In addition to the wind-driven mechanism, the aforementioned anomalous cooling introduced by the oceanic tunnel can reinforce and extend the intensified STC via altering density and vertical stability (53). The strengthened northern STC reaches its peak at year 10 and persists for more than 10 y after switching off aerosol emissions, leading to a continued export of energy and a gradually intensified cooling in the equatorial region (54). The cooler equatorial water is upwelled from the cold tongue, kicking off a series of air–sea interactions and leading to a persistent La Niña-like condition.

Summary and Outlook

We have examined the fast and slow components of tropical Pacific SST responses to anthropogenic sulfate aerosol emissions. We observe that the equatorial Pacific displays opposing signs of fast and slow components, and both components are insensitive to exact aerosol distributions outside the equatorial region. As summarized in Fig. 6, the unique patterns of both surface fast and subsurface slow responses reinforce each other, resulting in a notably strong equatorial cooling that persists decades after the removal of anthropogenic aerosols. Following an abrupt removal of aerosols, the Hadley Cell responds quickly (Figs. 5*A* and 6*A*). The intensified trades, the associated coastal Ekman upwelling, and the chain of low cloud-WES feedback processes, lead to a cooling trend in the southeast Pacific extending toward the equatorial central Pacific. The anomalous northern STC, which is the signature of the slow response of aerosol increase, persists for a few more years after the aerosol removal (Figs. 5*B* and 6*B*). This, in turn, results in a continued cooling trend in the equatorial subsurface. The surface air–sea interactions associated with the rapid Hadley Cell adjustment and the prolonged anomalous energy transport divergence in the ocean interior caused by the continuous northern STC strengthening both contribute constructively to the La Niña-like condition.

The characteristics of the two distinct components of response can be seen in simulations conducted under more realistic conditions, as well as in the observed trend. The fast response, which lasts only a few years in the idealized experiment, transforms into a continuous linear trend in the simulations with realistic aerosol emission trajectories, which exhibit increasing and decreasing trends lasting for decades. Notably, the greatest spatial correlation between the fast component identified in the idealized experiment and the linear trends observed in the CESM LE single forcing experiment is found during the 1960s—a decade marked by a substantial increase in Northern Hemisphere aerosol emissions (*SI Appendix*, Fig. S7). Conversely, La Niña-like trends emerge in the 1990s, coinciding with a more pronounced reduction in aerosol emissions in the CESM LE single forcing experiment. During 1981 to 2000, the period characterized by rapid interhemispherically asymmetric changes in SST, the spatial correlation between the fast component and the observed SST trend reaches −0.63 (*SI Appendix*, Fig. S7). Furthermore, the persistent cooling of the equatorial subsurface—a characteristic feature of the slow response—can be seen not only in the single forcing experiment but also in the standard historical simulation considering GHG warming and the reanalysis data (*SI Appendix*, Fig. S8).

Our findings are based on a single model (CESM), and the temporal and spatial characteristics of the two components identified here remain to be tested and compared with other models

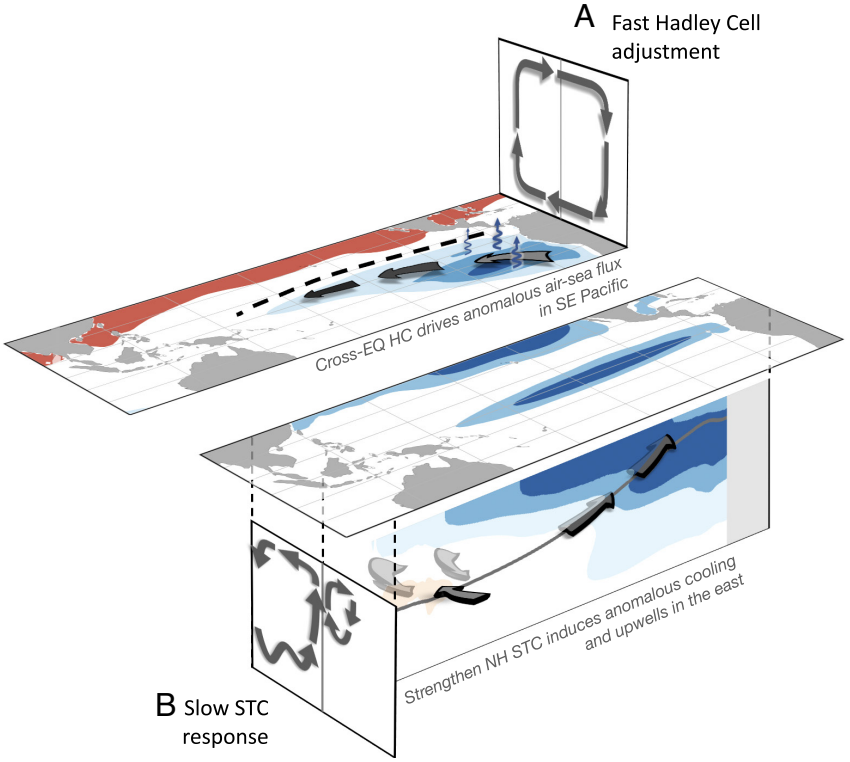

Fig. 6. A schematic illustrating the distinct characteristics of and the interplay between the fast component of aerosol emission reduction and the slow component of aerosol emission increase. Shadings represent anomalous oceanic potential temperature. Arrows in the two vertical planes are the anomalous cross-equatorial Hadley Cell and the anomalous oceanic STC. The thick arrows in the *Top* panel A illustrates intensified trades and the thin blue arrows illustrate the associated air-sea fluxes. The thick arrows in the *Bottom* panel B illustrate how the intensified STC induces cold water, which converges in west Pacific subtropics and upwells in the east.

and different emission scenarios. Despite the caveat, the mechanistic understanding of the two components reported here provides valuable insights for unraveling the discrepancies between global climate model simulations and observational records. For instance, the well-known double ITCZ biases, characterized by the presence of the eastern Pacific rainband in the southern hemisphere for a longer duration compared to the real world, can hinder the connection between the southern subtropics and the equatorial region in the fast component. In some global climate models, the spurious rainband obstructs the chain of air–sea interaction that typically brings the anomalous cooling from the South Pacific to the equatorial region. Furthermore, the underestimation of the strength of the stratus cloud-SST feedback, a bias common to most global climate models [but not the two-degree CESM1 that we use (35)], also impacts the relationship between SSTs in the southeast and equatorial Pacific. Turning to the slow response, biased low stratus cloud-SST feedbacks in the northern subtropics contribute to an inaccurate estimation of weakening in the STC and the resulting equatorial cooling. Additionally, global climate models tend to exhibit excessive stratification in the equatorial Pacific, impeding the upwelling of STC-induced cooling in the eastern equatorial Pacific. A process-based understanding of model biases is crucial for improved regional climate projections.

The implications of the proposed Hadley circulation and STC responses to an interhemispheric thermal gradient extend beyond the simulated effects of anthropogenic sulfate aerosols. The intensified warming trend observed in the mid-to-high latitudes of the Northern Hemisphere and the muted warming in the Southern Ocean, regardless of whether the causes are aerosol recovery, greenhouse gas-induced warming, or ozone depletion, could potentially trigger similar adjustments in the Hadley Cell, air–sea interaction, and STC. Although our study primarily focuses on the prolonged La Niña-like cooling trend, the accelerated warming over the Southern Ocean and the subtropical oceanic interior would engender a reverse mechanism and an El Niño-like background state in the future. Additionally, the circulation adjustments across multiple timescales and their impacts on the mean state of the tropical Pacific will also influence tropical climate variability, such as the El Niño/Southern Oscillation.

Methods

Definitions of the Fast and Slow Components. We define the fast components as the average of years 1 to 3 minus control and the average of years 31 to 35 minus years 11 to 20 (Fig. 3*A* and *SI Appendix*, Fig. S1*C*), based on the evolution of the Niño 3.4 index (Fig. 2*A*). The slow components are defined as the average of years 11 to 20 minus years 1 to 3 and the average of years 41 to 60 minus years 31 to 35 (Fig. 3*B* and *SI Appendix*, Fig. S1*E*). Through subtracting the fast component, the slow component partly excludes the cross-equatorial Hadley Cell response that develops quickly and highlights the enhanced equatorial response that is hemispherically symmetric. The overall patterns are not sensitive to the choice of the definitions, although the absolute anomalies are.

CESM Single Forcing Large Ensemble. To evaluate the climate responses to aerosol forcing with realistic temporal and spatial variations, we take the difference between the 40-member CESM large ensemble all forcing experiment (55) and the 20-member "XAERindus" experiment from the CESM single forcing large ensemble (29). The "XAERindus" uses the same forcing protocol as the all forcing experiment, i.e., the CMIP5 historical and RCP8.5 forcing protocols, except that the industrial anthropogenic aerosols' emission is held fixed at 1920 conditions. The model used in the CESM all forcing and single forcing large ensemble is the same as that of the idealized step function aerosol experiment used in this study but at a higher resolution (1°).

Data, Materials, and Software Availability. All processed data to support the analysis and figure codes publicly available at https://doi.org/10.6084/m9.figshare.24581016 (56). Data from CESM1 Single Forcing Large Ensemble Project is publicly available at: https://www.cesm.ucar.edu/working-groups/climate/simulations/cesm1-single-forcing-le (29). Monthly outputs from the idealized aerosol experiments are available from Y.-T.H. on request.

ACKNOWLEDGMENTS. S.-P.X. is sponsored by NSF AGS 2105654, C.D. by the NSF under Cooperative Agreement 1852977. Y.-T.H., P.-J.C., and H.-Y.T. are supported by Ministry of Science and Technology of Taiwan (MOST 110-2628-M-002-002, MOST 111-2628-M-002-003-, and NSTC 112-2111-M-002-016-MY4). We thank Hsing-Hung Chou for making the schematic (Fig. 6), Po-Chun Chung and Wan-Yu Wu for their help at the initial stage of the project, Kun Wang for sharing the codes for budget analysis, M.J.M. and K.M. for their constructive comments, and John Chiang and Yu-Heng Tseng for valuable discussions.

1. R. C. J. Wills, Y. Dong, C. Proistosecu, K. C. Armour, D. S. Battisti, Systematic climate model biases in the large-scale patterns of recent sea-surface temperature and sea-level pressure change. *Geophys. Res. Lett.* **49**, e2022GL100011 (2022).
2. Y. Kosaka, S.-P. Xie, Recent global-warming hiatus tied to equatorial Pacific surface cooling. *Nature* **501**, 403–407 (2013).
3. T. Andrews *et al.*, On the effect of historical SST patterns on radiative feedback. *J. Geophys. Res. Atmos.* **127**, e2022JD036675 (2022).
4. C. Zhao *et al.*, Enlarging rainfall area of tropical cyclones by atmospheric aerosols. *Geophys. Res. Lett.* **45**, 8604–8611 (2018).
5. R. Seager *et al.*, Causes of the 2011–14 California drought. *J. Clim.* **28**, 6997–7024 (2015).
6. S. Lee *et al.*, On the future zonal contrasts of equatorial Pacific climate: Perspectives from observations, simulations, and theories. *npj Clim. Atmos. Sci.* **5**, 82 (2022).
7. U. K. Heede, A. V. Fedorov, N. J. Burls, Time scales and mechanisms for the tropical Pacific response to global warming: A tug of war between the ocean thermostat and weaker walker. *J. Clim.* **33**, 6101–6118 (2020).
8. M. H. England *et al.*, Recent intensification of wind-driven circulation in the Pacific and the ongoing warming hiatus. *Nat. Clim. Change* **4**, 222–227 (2014).
9. M. Watanabe, J.-L. Dufresne, Y. Kosaka, T. Mauritsen, H. Tatebe, Enhanced warming constrained by past trends in equatorial Pacific sea surface temperature gradient. *Nat. Clim. Change* **11**, 33–37 (2021).
10. S. McGregor *et al.*, Recent Walker circulation strengthening and Pacific cooling amplified by Atlantic warming. *Nat. Clim. Change* **4**, 888–892 (2014).
11. G. Li, S.-P. Xie, Y. Du, Y. Luo, Effects of excessive equatorial cold tongue bias on the projections of tropical Pacific climate change. Part I: The warming pattern in CMIP5 multi-model ensemble. *Clim. Dyn.* **47**, 3817–3831 (2016).
12. G. A. Meehl, A. Hu, H. Teng, Initialized decadal prediction for transition to positive phase of the Interdecadal Pacific Oscillation. *Nat. Commun.* **7**, 11718 (2016).
13. S. Po-Chedley *et al.*, Natural variability contributes to model–satellite differences in tropical tropospheric warming. *Proc. Natl. Acad. Sci. U.S.A.* **118**, e2020962118 (2021).
14. S. Power *et al.*, Decadal climate variability in the tropical Pacific: Characteristics, causes, predictability, and prospects. *Science* **374**, eaay9165 (2021).
15. M. Newman *et al.*, The Pacific decadal oscillation. Revisited. *J. Clim.* **29**, 4399–4427 (2016).
16. T. R. Ault, C. Deser, M. Newman, J. Emile-Geay, Characterizing decadal to centennial variability in the equatorial Pacific during the last millennium. *Geophys. Res. Lett.* **40**, 3450–3456 (2013).
17. I. M. Held *et al.*, Probing the fast and slow components of global warming by returning abruptly to preindustrial forcing. *J. Clim.* **23**, 2418–2427 (2010).
18. S.-M. Long, S.-P. Xie, X.-T. Zheng, Q. Liu, Fast and slow responses to global warming: Sea surface temperature and precipitation patterns. *J. Clim.* **27**, 285–299 (2014).
19. U. K. Heede, A. V. Fedorov, N. J. Burls, A stronger versus weaker Walker: Understanding model differences in fast and slow tropical Pacific responses to global warming. *Clim. Dyn.* **57**, 2505–2522 (2021).
20. U. K. Heede, A. V. Fedorov, Colder eastern equatorial Pacific and stronger walker circulation in the early 21st century: Separating the forced response to global warming from natural variability. *Geophys. Res. Lett.* **50**, e2022GL101020 (2023).
21. A. C. Clement, R. Seager, M. A. Cane, S. E. Zebiak, An ocean dynamical thermostat. *J. Clim.* **9**, 2190–2196 (1996).
22. I. M. Held, B. J. Soden, Robust responses of the hydrological cycle to global warming. *J. Clim.* **19**, 5686–5699 (2006).
23. T. R. Knutson, S. Manabe, Time-mean response over the tropical pacific to increased CO2 in a coupled ocean-atmosphere model. *J. Clim.* **8**, 2181–2199 (1995).
24. S.-P. Xie *et al.*, Global warming pattern formation: Sea surface temperature and rainfall. *J. Clim.* **23**, 966–986 (2010).
25. R. Seager *et al.*, Strengthening tropical Pacific zonal sea surface temperature gradient consistent with rising greenhouse gases. *Nat. Clim. Change* **9**, 517–522 (2019).
26. C. Takahashi, M. Watanabe, Pacific trade winds accelerated by aerosol forcing over the past two decades. *Nat. Clim. Change* **6**, 768–772 (2016).
27. D. M. Smith *et al.*, Role of volcanic and anthropogenic aerosols in the recent global surface warming slowdown. *Nat. Clim. Change* **6**, 936–940 (2016).
28. U. K. Heede, A. V. Fedorov, Eastern equatorial Pacific warming delayed by aerosols and thermostat response to CO2 increase. *Nat. Clim. Change* **11**, 696–703 (2021).
29. C. Deser *et al.*, Isolating the evolving contributions of anthropogenic aerosols and greenhouse gases: A new CESM1 large ensemble community resource. *J. Clim.* **33**, 7835–7858 (2020).
30. S. M. Kang, S.-P. Xie, C. Deser, B. Xiang, Zonal mean and shift modes of historical climate response to evolving aerosol distribution. *Sci. Bull.* **66**, 2405–2411 (2021).
31. M. B. Menary *et al.*, Aerosol-forced AMOC changes in CMIP6 historical simulations. *Geophys. Res. Lett.* **47**, e2020GL088166 (2020).
32. B. B. B. Booth, N. J. Dunstone, P. R. Halloran, T. Andrews, N. Bellouin, Aerosols implicated as a prime driver of twentieth-century North Atlantic climate variability. *Nature* **484**, 228–232 (2012).
33. T. Verma, R. Saravanan, P. Chang, S. Mahajan, Tropical pacific ocean dynamical response to short-term sulfate aerosol forcing. *J. Clim.* **32**, 8205–8221 (2019).
34. B. L. Otto-Bliesner *et al.*, Climate variability and change since 850 CE: An ensemble approach with the community earth system model. *Bull Am. Meteorol. Soc.* **97**, 735–754 (2016).
35. H. Kim, S. M. Kang, J. E. Kay, S.-P. Xie, Subtropical clouds key to Southern Ocean teleconnections to the tropical Pacific. *Proc. Natl. Acad. Sci. U.S.A.* **119**, e2200514119 (2022).
36. Y. Y. Planton *et al.*, Evaluating climate models with the CLIVAR 2020 ENSO metrics package. *Bull Am. Meteorol. Soc.* **102**, E193–E217 (2021).
37. S. M. Kang, I. M. Held, D. M. W. Frierson, M. Zhao, The response of the ITCZ to extratropical thermal forcing: Idealized slab-ocean experiments with a GCM. *J. Clim.* **21**, 3521–3532 (2008).
38. T. Schneider, T. Bischoff, G. H. Haug, Migrations and dynamics of the intertropical convergence zone. *Nature* **513**, 45–53 (2014).
39. Y.-T. Hwang, D. M. W. Frierson, S. M. Kang, Anthropogenic sulfate aerosol and the southward shift of tropical precipitation in the late 20th century. *Geophys. Res. Lett.* **40**, 2845–2850 (2013).
40. S. Hu, A. V. Fedorov, Cross-equatorial winds control El Niño diversity and change. *Nat. Clim. Change* **8**, 798–802 (2018).
41. F. S. R. Pausata, D. Zanchettin, C. Karamperidou, R. Caballero, D. S. Battisti, ITCZ shift and extratropical teleconnections drive ENSO response to volcanic eruptions. *Sci. Adv.* **6**, eaaz5006 (2020).
42. M. E. Mann, M. A. Cane, S. E. Zebiak, A. Clement, Volcanic and solar forcing of the tropical pacific over the past 1000 years. *J. Clim.* **18**, 447–456 (2005).
43. H. Zhang, C. Deser, A. Clement, R. Tomas, Equatorial signatures of the pacific meridional modes: Dependence on mean climate state. *Geophys. Res. Lett.* **41**, 568–574 (2014).
44. Y.-T. Hwang, S.-P. Xie, C. Deser, S. M. Kang, Connecting tropical climate change with Southern Ocean heat uptake. *Geophys. Res. Lett.* **44**, 9449–9457 (2017).
45. S. M. Kang *et al.*, Walker circulation response to extratropical radiative forcing. *Sci. Adv.* **6**, eabd3021 (2020).
46. W.-T. Hsiao, Y.-T. Hwang, Y.-J. Chen, S. M. Kang, The role of clouds in shaping tropical pacific response pattern to extratropical thermal forcing. *Geophys. Res. Lett.* **49**, e2022GL098023 (2022).
47. H.-Y. Tseng *et al.*, Fast and slow responses of the tropical pacific to radiative forcing in northern high latitudes. *J. Clim.* **36**, 1–31 (2023).
48. S.-P. Xie *et al.*, Similar spatial patterns of climate responses to aerosol and greenhouse gas changes. *Nat. Geosci.* **6**, 828–832 (2013).
49. N. J. Burls, L. Muir, E. M. Vincent, A. Fedorov, Extra-tropical origin of equatorial Pacific cold bias in climate models with links to cloud albedo. *Clim. Dyn.* **49**, 2093–2113 (2017).
50. Z. Liu, B. Huang, A coupled theory of tropical climatology: Warm pool, cold tongue, and walker circulation. *J. Clim.* **10**, 1662–1679 (1997).
51. A. Capotondi, B. Qiu, Decadal variability of the pacific shallow overturning circulation and the role of local wind forcing. *J. Clim.* **36**, 1001–1015 (2023).
52. A. Capotondi, M. A. Alexander, C. Deser, M. J. McPhaden, Anatomy and decadal evolution of the pacific subtropical-tropical cells (STCs). *J. Clim.* **18**, 3739–3758 (2005).
53. M. T. Luongo, S.-P. Xie, I. Eisenman, Buoyancy forcing dominates the cross-equatorial ocean heat transport response to northern hemisphere extratropical cooling. *J. Clim.* **35**, 6671–6690 (2022).
54. M. J. McPhaden, D. Zhang, Pacific Ocean circulation rebounds. *Geophys. Res. Lett.* **31**, L18301 (2004).
55. J. E. Kay *et al.*, The community earth system model (CESM) large ensemble project: A community resource for studying climate change in the presence of internal climate variability. *Bull Am. Meteorol. Soc.* **96**, 1333–1349 (2015).
56. H.-Y. Tseng, Data for PNAS 2023. Figshare. https://doi.org/10.6084/m9.figshare.24581016. Deposited 17 November 2023.